Journal of Materials Chemistry A

COMMUNICATION

View Article Online
View Journal | View Issue

Cite this: J. Mater. Chem. A, 2016, 4, 9002

Received 26th April 2016
Accepted 16th May 2016

DOI: 10.1039/c6ta03477b

www.rsc.org/MaterialsA

A fiber-shaped aqueous lithium ion battery with high power density†

Ye Zhang,[a] Yuhang Wang,[b] Lie Wang,[a] Chieh-Min Lo,[a] Yang Zhao,[a] Yiding Jiao,[a] Gengfeng Zheng[b] and Huisheng Peng*[a]

A new fiber-shaped aqueous lithium ion battery is developed using a polyimide/carbon nanotube hybrid fiber as the anode and $LiMn_2O_4$/carbon nanotube hybrid fiber as the cathode. This battery outputs a power density of 10 217.74 W kg^{-1}, which exceeds that of most supercapacitors, and an energy density of 48.93 W h kg^{-1}, which equals that of thin-film lithium ion batteries. The safety issue generated by flammable organic electrolytes is fundamentally resolved by using an aqueous electrolyte. Compared with the conventional planar structure, the fiber shape also provides some unique and promising advantages, *e.g.*, being three-dimensionally deformable. It can be also woven into a flexible power textile to satisfy a variety of new emerging fields, such as microelectronics and wearable electronics.

Introduction

An enormous challenge facing energy storage devices is the achievement of high power output while maintaining high energy storage capacity.[1–3] Lithium ion batteries deliver high energy densities through faradaic reactions, but are plagued by sluggish charge/discharge processes and low power densities.[4,5] Supercapacitors conduct fast charge/discharge processes through surface ion adsorptions or surface redox reactions, thus exhibiting higher power densities. However, they suffer from lower energy densities compared with lithium ion batteries.[6–8] Considerable efforts have been made to enhance the power densities of lithium ion batteries by shortening the diffusion distances of lithium ions[9,10] and increasing the energy densities of supercapacitors by designing electrode materials with high specific surface areas, high pseudocapacitances, or both.[11–13] However, the improvement of these properties by bridging the gap between batteries and supercapacitors is limited.

On the other hand, flexible and wearable electronics represent a promising future trend,[14] and their rapid advancement requires energy storage devices with more rigorous criteria, including miniaturization, nontoxicity, high safety and flexibility.[15,16] Numerous attempts have thus been made to develop matching power systems. However, the available flexible lithium ion batteries are based on flammable and toxic organic electrolytes; thus, they suffer from risks of fires and explosions caused by short circuiting during deformation, which is a key challenge that has hindered their potential applications.[17]

Herein, a fiber-shaped aqueous lithium ion battery (FAL) is created with excellent electrochemical properties by designing a polyimide (PI)/carbon nanotube (CNT) hybrid fiber as the anode, a $LiMn_2O_4$ (LMO)/CNT hybrid fiber as the cathode, and lithium sulfate aqueous solution as the electrolyte. The PI/CNT anode achieved superior rate capability and high specific capacity that was maintained at 86 mA h g^{-1} even at a high current rate of 600C. Reports of such a high rate performance are rare. The fabricated FAL afforded a power density of 10 217.74 W kg^{-1}, which is superior to that of most supercapacitors, and an energy density of 48.93 W h kg^{-1}, which is comparable to that of thin-film lithium ion batteries. Furthermore, the safety issues derived from flammable organic electrolytes were fundamentally resolved by using an aqueous electrolyte. The one-dimensional fiber shape allows the FAL to be deformable in all directions. As a demonstration for large-scale applications, it was further woven into a flexible battery textile to meet the requirements of a variety of new emerging applications, such as electronic skins.

Experimental section

Fabrication of electrodes

To prepare the PI/CNT hybrid fiber electrode, 1,4,5,8-naphthalenetetracarboxylic dianhydride (2.3 mmol) was first mixed

[a]State Key Laboratory of Molecular Engineering of Polymers, Collaborative Innovation Center of Polymers and Polymer Composite Materials, Department of Macromolecular Science and Laboratory of Advanced Materials, Fudan University, Shanghai 200438, China. E-mail: penghs@fudan.edu.cn

[b]Laboratory of Advanced Materials, Department of Chemistry, Collaborative Innovation Center of Chemistry for Energy Materials, Fudan University, Shanghai 200433, China

† Electronic supplementary information (ESI) available. See DOI: 10.1039/c6ta03477b

with *p*-chlorophenol (40 g), followed by addition of ethylene diamine (0.15 mL). Aligned CNT fiber spun from a spinnable CNT array was then immobilized in the precursor solution, followed by heating and refluxing for 2, 6 or 8 h. The obtained hybrid fiber was rinsed with ethanol and dried at 300 °C in N_2 for 8 h to remove residual solvent. The weight percentages of PI with a growing time of 6 h in the hybrid fiber were measured as 53%. The PI powder was synthesized *via* the same procedure, but without CNT fiber. To prepare the LMO/CNT hybrid fiber electrode, LMO (2.25 mg) synthesized *via* a hydrothermal method[18] was first dispersed in *N*,*N*-dimethylformamide (15 mL), and ten stacked CNT sheets drawn from a spinnable CNT array were then immersed in the LMO suspension. The resulting hybrid sheet was scrolled into an LMO/CNT fiber. The weight percentages of LMO in the hybrid fibers were measured as 49%. The loading content of LMO in the hybrid fiber was determined by the concentration of LMO/*N*,*N*-dimethylformamide suspension, *e.g.*, 49% for 0.15 mg mL^{-1}, 56% for 0.2 mg mL^{-1} and 91.7% for 0.5 mg mL^{-1}.

Fabrication of FAL

The above two hybrid fibers were paired with a separator and inserted into a heat-shrinkable tube. After purging with argon gas for 2 h, an aqueous Li_2SO_4 solution (0.5 M) was used as the electrolyte and injected into the tube. The full FAL was finally sealed using a heat gun at 120 °C for 1 min.

Calculation

The specific capacity (C) of the fiber electrode was calculated from the equation of $C = (I \times t)/m$, where I, t, and m correspond to the applied current, discharge time and mass of active materials, respectively. The mass of active materials can be obtained from the total mass of fiber electrode minus the mass of CNT. For instance, the mass of pure CNT with a length of 5 cm was 0.049 mg. After *in situ* polymerization of PI, the mass was 0.105 mg; thus, the mass of PI was 0.056 mg. After loading LMO, the mass of the LMO/CNT hybrid fiber was 0.096 mg; thus, the mass of LMO was 0.047 mg. The energy density (E) based on the electrodes was calculated from $E_V = (I \times U \times t)/V$ or $E_M = (I \times U \times t)/M$, and the power density (P) based on the electrodes was obtained from $P_V = (I \times U)/V$ or $P_M = (I \times U)/M$, where I, U, t, V and M represent the applied current, average operating voltage, discharge time, volume and mass of the two hybrid fiber electrodes, respectively. The energy density ($E_{battery}$) and power density ($P_{battery}$) based on the device were calculated from $E_{battery} = (I \times U \times t)/M_{battery}$ and $P_{battery} = (I \times U)/M_{battery}$, where $M_{battery}$ represents the total mass of the FAL, including the PI, LMO, CNT, electrolyte and package material.

Results and discussion

Two different electrode structures were designed to incorporate the active materials. CNT fiber with a uniform diameter along the length direction was first spun from a CNT array synthesized by chemical vapor deposition[19] (Fig. S1†); the diameters of the CNT fibers were controlled by varying the width of the spun CNT, typically from several to tens of micrometers. The fabricated CNTs were highly aligned (Fig. S2†) along the spiral direction, thereby providing the resulting fiber with high electrical conductivities at the order of 10^2 to 10^3 S cm^{-1} and tensile strengths on the level of 10^2 to 10^3 MPa.[20] PI was coated onto the surface of aligned CNT fiber by *in situ* polymerization to form a skin–core structure. After the formation of the hybrid fiber, the aligned structure and the mechanical properties were well maintained, and the diameter of the hybrid fiber slightly increased (Fig. 1a, b and S3†). PI nanosheets with widths of ~300 nm and thicknesses of ~25 nm were uniformly coated on the CNT fiber. Interestingly, the PI nanosheets were perpendicularly grown on the surface of the CNT fiber substrate with numerous voids between them (Fig. 1c). With a further increase in polymerization time from 6 to 8 h, the PI nanosheets were closely stacked and fused into a dense layer without voids for infiltration to the inner CNT (Fig. 1d). The formation of PI on the CNT fiber was verified by Fourier transform infrared spectroscopy (Fig. S4†). The peak at 1350 cm^{-1} is ascribed to the stretching vibration of the C–N bond, and the peaks at 767, 1670 and 1700 cm^{-1} are assigned to the C=O bond.[21]

The cathode was prepared by incorporating LMO nanoparticles into the aligned CNT fibers through a co-spinning process.[22] The LMO nanoparticles, with an average diameter of ~200 nm, exhibited a spinel structure, which was validated by the X-ray diffraction patterns (Fig. S5 and S6†). An LMO suspension was dropped onto the CNT sheets, followed by twisting into a hybrid fiber. The LMO nanoparticles were well wrapped by the CNT (Fig. 1e and f).

The hybrid PI/CNT and LMO/CNT hybrid fibers were highly flexible, and no obvious damage in structure was observed for

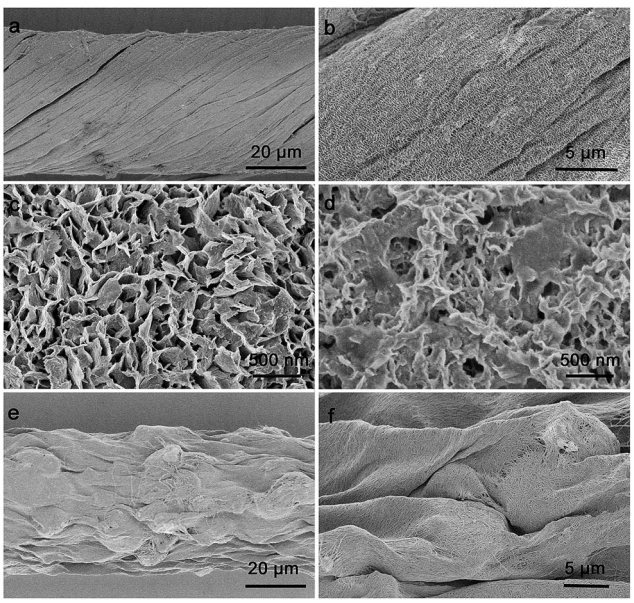

Fig. 1 Scanning electron microscopy (SEM) images of PI/CNT and LMO/CNT hybrid fibers. (a–c) A PI/CNT hybrid fiber with a PI growth time of 6 h at different magnifications. (d) A PI/CNT hybrid fiber with a PI growth time of 8 h. (e and f) An LMO/CNT hybrid fiber at low and high magnification, respectively.

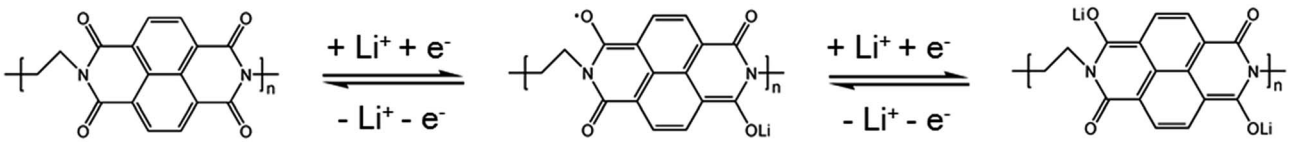

Scheme 1 Electrochemical redox reactions of lithium ions with PI.

both of them after bending for 1000 cycles (Fig. S7†). The electrical resistances of the two fibers were further traced during the bending process to verify the structural integrity (Fig. S8 and S9†). The electrical resistances of both the PI/CNT and LMO/CNT hybrid fibers varied less than 5% after bending for 1000 cycles.

The electrochemical performance of the hybrid fibers were investigated in a three-electrode cell in 0.5 M Li_2SO_4. PI was chosen as the active anode material in the present aqueous lithium ion battery due to its high energy storage capacity and suitable redox voltage. PI possesses conjugated carbonyl groups which can store energy through a two-step redox process. As shown in Scheme 1, during the reduction process, PI first transforms into the radical anion ($PI^{\bullet -}$) and then the dianion (PI^{2-}) along with the incorporation of lithium ions. This process was reversed in the oxidation process.[21,23] Additionally, as shown in the CV curve (Fig. S10†), the redox voltages of PI were located at around −0.8 V and −0.6 V *versus* a saturated calomel electrode (2.2 V and 2.4 V *vs.* Li^+/Li); these fall into the range of the evolution potential between O_2 and H_2 in an aqueous electrolyte. Therefore, PI is suitable for aqueous systems.

We first compared the specific capacities of PI/CNT hybrid fibers with different PI growth times. The specific capacities increased with increasing growth time from 0 to 6 h and then decreased with a further increase in growth time (Fig. S11†). The decreasing specific capacity was mainly derived from the fact that PI nanosheets were aggregated into a relatively dense layer at higher growth times, and it was difficult for the electrolyte to infiltrate into the conductive CNT core; thus, the inner PI layer could not be effectively used. Therefore, an optimal growth time of 6 h was explored in the following discussion. Note that the bare CNT fiber showed almost no capacity in the voltage range from −1.0 V to 0 V *versus* a saturated calomel electrode (Fig. S12†); therefore, the energy storage capacity was mainly derived from the redox reaction of PI.

The PI/CNT hybrid fiber delivered a specific capacity of 144 mA h g^{-1} at a rate of 1C (Fig. S13†). The rate of 1C corresponds to a full discharge of 1 h, which is based on the theoretical capacity of 183 mA h g^{-1} for PI. Thus, the rate of 1C indicates a charge and discharge current density of 183 mA g^{-1}. The PI/CNT hybrid fiber showed two discharge voltage platforms at appropriately −0.6 and −0.8 V *versus* the saturated calomel

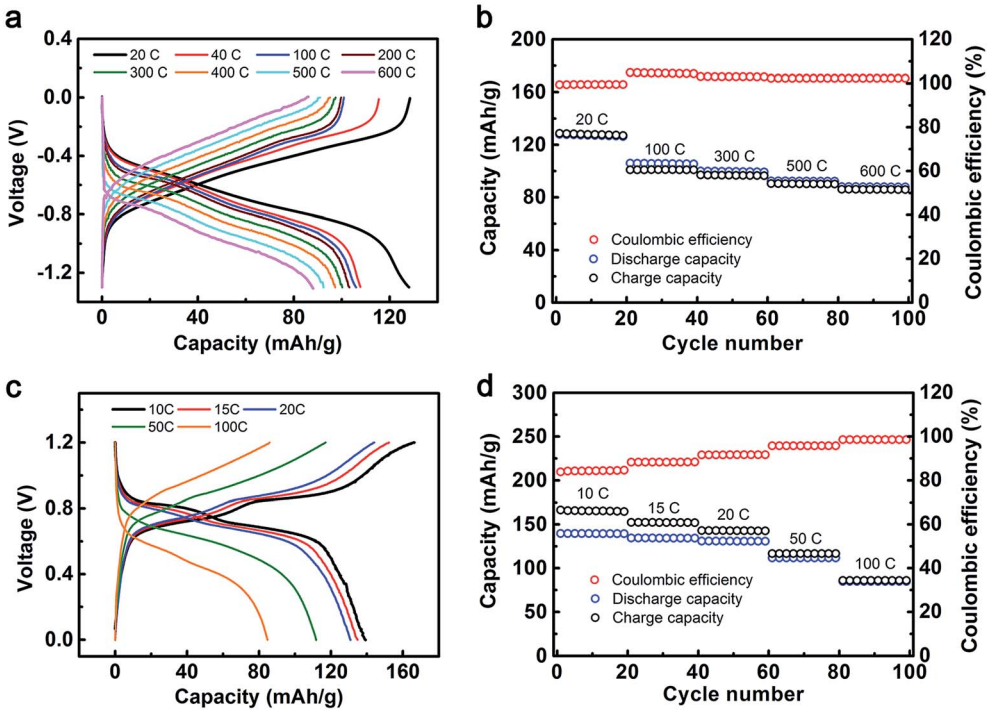

Fig. 2 Electrochemical performance of the PI/CNT and LMO/CNT fiber electrodes. (a and b) Charge–discharge curves and rate capability of the PI/CNT fiber anode under increasing current rates (1C = 183 mA g^{-1}), respectively. (c and d) Charge–discharge curves and rate capability of the LMO/CNT fiber cathode under increasing current rates (1C = 148 mA g^{-1}), respectively.

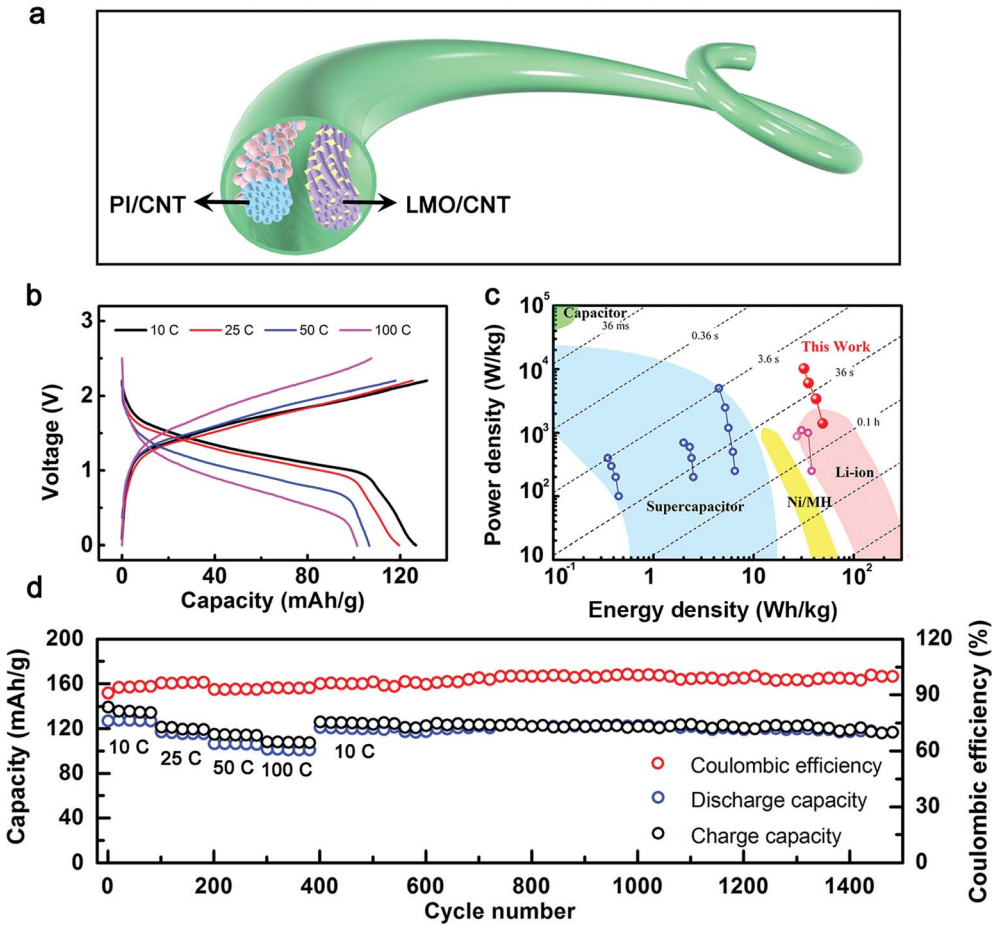

Fig. 3 Schematic and electrochemical performance of the FAL. (a) Schematic illustration of a simplified structure of the FAL showing only the two hybrid electrodes (*i.e.*, PI/CNT and LMO/CNT). (b) Charge and discharge curves of the FAL under increasing current rates (1C = 183 mA g^{-1}). (c) Energy and power densities of the FAL compared with previous energy storage systems. (d) Rate performance at increasing current rates from 10 to 100C and long-term stability test of the FAL at a current rate of 10C.

electrode. We further investigated the rate performance of the PI/CNT fiber electrode at rates ranging from 20 to 600C (Fig. 2a and b). The PI/CNT hybrid fiber delivered a specific capacity of 129.8 mA h g^{-1} at a rate of 20C. Even at a high charge and discharge rate of 600C, the fiber still retained a specific capacity of 86 mA h g^{-1}, corresponding to 60% of the specific capacity at 1C. Table S1† compares the performance of the PI/CNT anode with reported representative anodes (*e.g.*, VO_2, $LiTi_2(PO_4)_3$, C–TiP_2O_7 and MoO_3/polypyrrole) in aqueous lithium ion batteries.[24–28] To the best of our knowledge, there are few reports on anode materials that can obtain such high capacities under both ultrafast charge and discharge rates. Additionally, the PI/CNT electrode demonstrated a stable cycling performance. More than 90% of the specific capacity was retained after 200 cycles at the rate of 20C, with a coulombic efficiency of ~100% (Fig. S14†).

The LMO/CNT hybrid fiber showed a specific capacity of 140 mA h g^{-1} at the rate of 10C (1C = 148 mA g^{-1}) with two discharge voltage plateaus of 0.7 and 0.8 V *versus* a saturated calomel electrode (Fig. 2c). Additionally, after 200 cycles at a current rate of 10C, the specific capacity was well maintained by over 90%, indicating high cycling stability (Fig. S15†). The LMO/CNT hybrid fiber electrode also exhibited an excellent rate performance, and discharge capacities were retained of 134.5 mA h g^{-1} at 15C, 131.0 mA h g^{-1} at 25C, 111.6 at 50C and 84.7 mA h g^{-1} at 100C (Fig. 2d). The excellent rate performance is derived from the nanostructure of LMO, which decreased the distance of Li^+ transport in the solid state.[29] As a comparison, the LMO nanoparticles were replaced by commercial LMO with a diameter of 1 μm, and the capacity decreased remarkably (Fig. S16 and S17†).

The two fiber electrodes were sealed in a heat-shrinkable tube to complete a full FAL, and the schematic illustration of the structure of FAL is shown in Fig. 3a. The full FAL exhibited a specific discharge capacity of 123 mA h g^{-1} based on the mass of PI and the discharge voltage platform of 1.4 V at the current rate of 10C (1C = 183 mA g^{-1}). Remarkably, the charge and discharge curves were well maintained under increasing current rates, and the specific capacity was 101 mA h g^{-1} even at a current rate of 100C (Fig. 3b). Additionally, the FAL also showed a high cyclic performance, and the specific capacity was well maintained for over 1000 cycles with a coulombic efficiency

of ~98% (Fig. 3d). The morphologies of PI/CNT and LMO/CNT hybrid electrodes remained almost unchanged after charging and discharging (Fig. S18 and S19†). The specific capacity can be well maintained at 105 mA h g^{-1} after the FAL is scaled up to a length of 200 mm at 10C (Fig. S20†). Furthermore, the FALs were demonstrated to lighten up light emitting diodes; we drilled through a FAL during use, and no safety hazard was observed, owing to the lack of flammable organic electrolyte (Movie S1†).

The energy and power densities are two important parameters for studying the electrochemical performance. Fig. 3c shows the Ragone plot, which was derived from the charge and discharge curves at current rates from 10 to 100C. The power density reached 10 217.7 W kg^{-1} or 2.98 W cm^{-3} based on the weight or volume of the two fiber electrodes. The FAL displayed an energy density up to 48.93 W h kg^{-1} or 14.30 mW h cm^{-3}.

The FAL exhibited a linear density of 10 mg m^{-1}. On the basis of the total mass of the FAL including the PI, LMO, CNT, electrolyte and package material, the power and energy densities were calculated as 3984.9 W kg^{-1} and 19.1 W h kg^{-1}, respectively. As shown in Table S2,† compared with the previous fiber-shaped organic lithium ion batteries, the FAL displayed ultrafast charge and discharge, and the power density of FAL was enhanced by ten to twenty times.[22,30] Additionally, the safety was greatly improved. The energy density of FAL was two to ten times higher than that of previously reported fiber-shaped supercapacitors, and the power density also surpassed that of most previously reported fiber-shaped supercapacitors.[7,15] Compared with the bulk aqueous lithium ion battery, the small-scale battery exhibited high rate performance, which is also an advantage of micro-devices. Additionally, the FAL showed higher power density, better cyclic stability and higher flexibility.[31,32]

The good electrochemical performance of the hybrid fiber electrode is due to its unique structure. Kinetics analysis was carried out for the PI/CNT anode and the LMO/CNT cathode *via* CV measurements. The CV curves for the cathode and anode exhibited similar shapes, with two broad peaks at increasing sweep rates from 1 to 10 mV s^{-1} during both the cathodic and anodic processes (Fig. 4a and S21†). According to the relationship equation between the current and sweep rate of $j = av^b$, the value of b can be calculated from the slope of a log(v)–log(j) plot.[33] Theoretically, for a b value of 0.5, the related electrochemical process is a diffusion-controlled process, whereas the value of 1.0 corresponds to an adsorption-controlled behavior. As shown in Fig. 4b, the b value for the redox peak of PI was 1.0, reflecting an adsorption-controlled electrochemical process.[6] Meanwhile, for $LiMn_2O_4$, the related b value was 0.67, indicting a diffusion-controlled behavior (Fig. S22†). The adsorption-controlled electrochemical process reflects capacitor-like properties;[34] therefore, PI dominates the extraordinary performance of this FAL. The rapid reaction through the PI/CNT hybrid fiber produced good electrochemical properties.

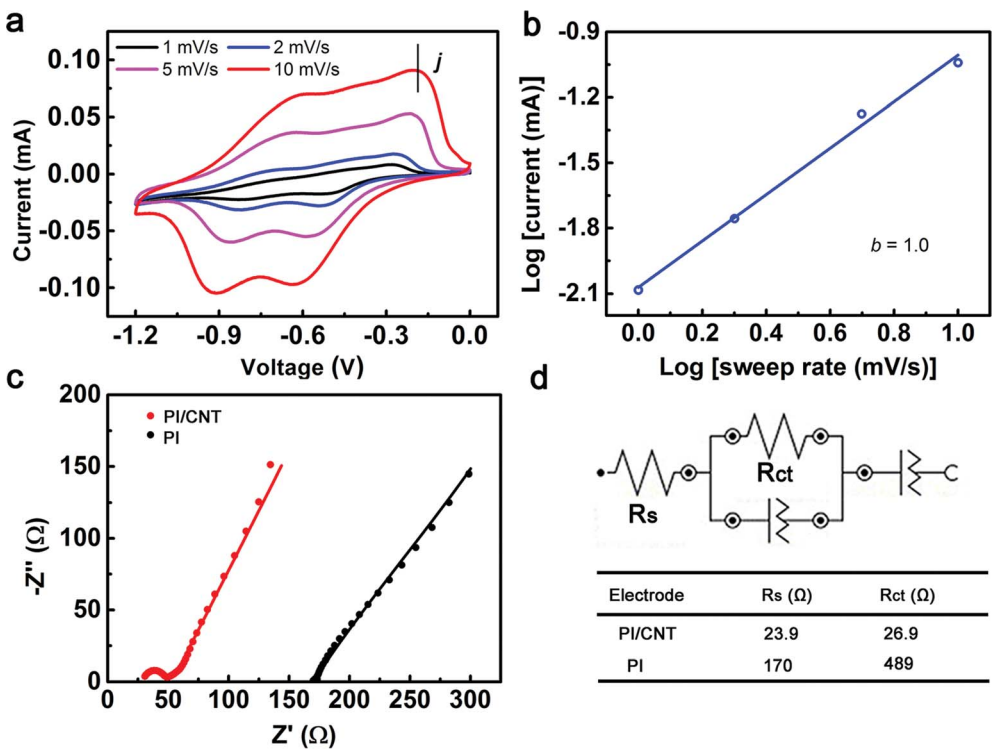

Electrode	Rs (Ω)	Rct (Ω)
PI/CNT	23.9	26.9
PI	170	489

Fig. 4 (a) CV curves of a PI/CNT fiber electrode at increasing scan rates. (b) Determination of the b value according to the relationship between sweep rate (mV s^{-1}) and current (mA) of the PI/CNT fiber electrode. (c) Electrochemical impedance spectroscopy of the PI and PI/CNT electrodes. (d) Equivalent circuit and corresponding parameters.

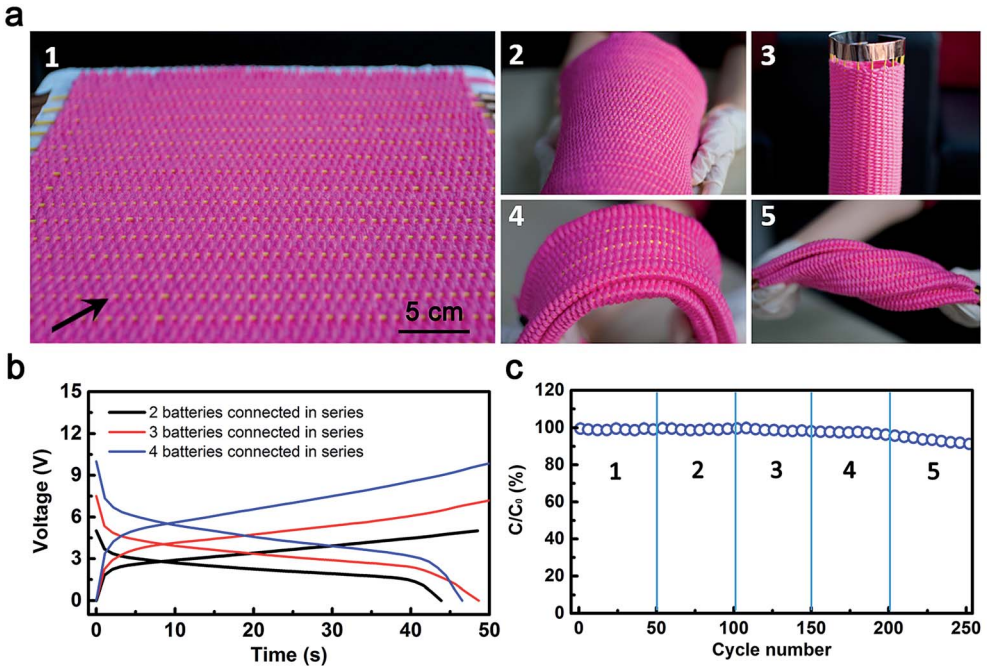

Fig. 5 FALs woven into textiles. (a) Energy textile woven with FALs under bending, folding and twisting. The numbers 1 to 5 correspond to the states before and after different deformations. The arrow at 1 indicates a FAL in the textile. (b) Galvanostatic charge and discharge curves of the FALs connected in series. (c) The capacity ratio of an energy textile under different conditions, shown at (a). C_0 and C correspond to the specific capacities before and after deformation of the energy textile, respectively.

PI is intrinsically insulative, and the aligned CNT fiber with high electrical conductivity guaranteed the efficient realization of its capacitor-like properties. The aligned CNT fiber not only acted as a strong and flexible skeleton to support active PI nanosheets and LMO nanoparticles, but also functioned as a current collector to ensure the rapid transport of electrons and ions. No binder, conductive agent or metal were required for the FAL. Meanwhile, PI nanosheets were grown *in situ* on the CNT fiber to ensure close contact between the two parts, and also for efficient charge transport. Additionally, the voids formed among PI nanosheets are beneficial for the infiltration of the electrolyte. Electrochemical impedance spectra were recorded for different electrode structures. For the PI/CNT fiber (red curve), the solution resistance (R_s) and charge transfer resistance (R_{ct}) were calculated as 23.9 Ω and 29.6 Ω, much lower than those of the electrode consisting of PI powder (black curve, 170 Ω and 489 Ω, respectively) (Fig. 4c and d). The cyclic voltammograms of the PI/CNT and PI electrodes were also conducted to compare the electrochemical performance (Fig. S23†). The smaller separation of the redox peaks and the larger peak area of the PI/CNT electrode indicated that the aligned CNTs facilitated smaller polarization. The full FAL was capable of achieving ultrafast charge and discharge.

This FAL can be continuously fabricated through a solution process and woven into various flexible structures, such as textiles, that can be bent, folded and twisted into various architectures (Fig. 5a). The FALs in the textile can be further connected in series; thus, the operating voltage can be enhanced from 2.5 V for a single FAL to 5, 7.5 and 10 V after connection of two, three and four ones, respectively (Fig. 5b). The electrochemical performance was also maintained under a variety of deformations (Fig. 5c).

Conclusion

To summarize, an environmentally friendly FAL with a novel fiber shape with good electrochemical performance was developed. Particularly, it displayed a high power density in addition to a high energy density, arising from the unique hybrid structure of the two fiber electrodes. In addition, the FALs were woven into flexible power textiles that represent a promising direction in the advancement of energy storage.

Acknowledgements

This work was supported by NSFC (21225417, 51573027, 51403038), STCSM (15XD1500400, 15JC1490200) and the Program for Outstanding Young Scholars from the Organization Department of the CPC Central Committee.

References

1 S. W. Lee, N. Yabuuchi, B. M. Gallant, S. Chen, B. S. Kim, P. T. Hammond and Y. S. Horn, *Nat. Nanotechnol.*, 2010, **5**, 531.
2 H. Zhang, X. Yu and P. V. Braun, *Nat. Nanotechnol.*, 2011, **6**, 277.
3 Y. Zhang, Y. Zhao, X. Cheng, W. Weng, J. Ren, X. Fang, Y. Jiang, P. Chen, Z. Zhang, Y. Wang and H. Peng, *Angew. Chem., Int. Ed.*, 2015, **54**, 11177.

4 H. Song, H. X. Wang, Z. Lin, X. Jiang, L. Yu, J. Xu, Z. Yu, X. Zhang, Y. Liu, P. He, L. Pan, Y. Shi, H. Zhou and K. Chen, *Adv. Funct. Mater.*, 2016, **26**, 524.
5 K. S. Kang, Y. S. Meng, J. Breger, C. P. Grey and G. Ceder, *Science*, 2006, **311**, 977.
6 P. Simon, Y. Gogotsi and B. Dunn, *Science*, 2014, **343**, 1210.
7 L. Kou, T. Huang, B. Zheng, Y. Han, X. Zhao, K. Gopalsamy, H. Sun and C. Gao, *Nat. Commun.*, 2014, **5**, 3754.
8 X. Yang, C. Cheng, Y. Wang, L. Qiu and D. Li, *Science*, 2013, **341**, 534.
9 J. Zheng, Y. Hou, Y. Duan, X. Song, Y. Wei, T. Liu, J. Hu, H. Guo, Z. Zhuo, L. Liu, Z. Chang, X. Wang, D. Zherebetskyy, Y. Fang, Y. Lin, K. Xu, L. W. Wang, Y. Wu and F. Pan, *Nano Lett.*, 2015, **15**, 6102.
10 Y. Wang, X. Xu, C. Cao, C. Shi, W. Mo and H. Zhu, *J. Power Sources*, 2013, **242**, 230.
11 N. Li, Z. Chen, W. Ren, F. Li and H. M. Cheng, *Proc. Natl. Acad. Sci. U. S. A.*, 2012, **109**, 17360.
12 R. B. Rakhi, W. Chen, D. Cha and H. N. Alshareef, *Nano Lett.*, 2012, **12**, 2559.
13 W. Gu, M. Sevilla, A. Magasinski, A. B. Fuertes and G. Yushin, *Energy Environ. Sci.*, 2013, **6**, 2465.
14 F. Zhao, Y. Zhao, H. Cheng and L. Qu, *Angew. Chem., Int. Ed.*, 2015, **54**, 14951.
15 D. Yu, K. Goh, H. Wang, L. Wei, W. Jiang, Q. Zhang, L. Dai and Y. Chen, *Nat. Nanotechnol.*, 2014, **9**, 555.
16 P. Huang, C. Lethien, S. Pinaud, K. Brousse, R. Laloo, V. Turq, M. Respaud, A. Demortière, B. Daffos and P. Taberna, *Science*, 2016, **351**, 691.
17 Y. Zhang, Y. Zhao, J. Ren, W. Weng and H. Peng, *Adv. Mater.*, 2015, DOI: 10.1002/adma.201503891.
18 Y. Y. Liang, S. J. Bao, B. L. He, W. J. Zhou and H. L. Li, *J. Electrochem. Soc.*, 2005, **152**, A2030.
19 Z. Zhang, K. Guo, Y. Li, X. Li, G. Guan, H. Li, Y. Luo, F. Zhao, Q. Zhang and B. Wei, *Nat. Photonics*, 2015, **9**, 233.
20 W. Guo, C. Liu, F. Zhao, X. Sun, Z. Yang, T. Chen, X. Chen, L. Qiu, X. Hu and H. Peng, *Adv. Mater.*, 2012, **24**, 5379.
21 Z. Song, H. Zhan and Y. Zhou, *Angew. Chem., Int. Ed.*, 2010, **49**, 8444.
22 W. Weng, Q. Sun, Y. Zhang, H. Lin, J. Ren, X. Lu, M. Wang and H. Peng, *Nano Lett.*, 2014, **14**, 3432.
23 H. Wu, S. A. Shevlin, Q. Meng, W. Guo, Y. Meng, K. Lu, Z. Wei and Z. Guo, *Adv. Mater.*, 2014, **26**, 3338.
24 F. Wang, Y. Liu and C. Liu, *Electrochim. Acta*, 2010, **55**, 2662.
25 Z. Liu, X. Qin, H. Xu and G. Chen, *J. Power Sources*, 2015, **293**, 562.
26 W. Wu, S. Shanbhag, A. Wise, J. Chang, A. Rutt and J. F. Whitacre, *J. Electrochem. Soc.*, 2015, **162**, A1921.
27 W. Tang, L. Liu, Y. Zhu, H. Sun, Y. Wu and K. Zhu, *Energy Environ. Sci.*, 2012, **5**, 6909.
28 C. Wessells, F. La Mantia, H. Deshazer, R. A. Huggins and Y. Cui, *J. Electrochem. Soc.*, 2011, **158**, A352.
29 N. C. Li, C. J. Patrissi, G. L. Che and C. R. Martin, *J. Electrochem. Soc.*, 2000, **147**, 2044.
30 J. Ren, Y. Zhang, W. Bai, X. Chen, Z. Zhang, X. Fang, W. Weng, Y. Wang and H. Peng, *Angew. Chem., Int. Ed.*, 2014, **126**, 7998.
31 J. Y. Luo and Y. Y. Xia, *Adv. Funct. Mater.*, 2007, **17**, 3877.
32 W. Tang, L. Liu, Y. Zhu, H. Sun, Y. Wu and K. Zhu, *Energy Environ. Sci.*, 2012, **5**, 6909.
33 V. Augustyn, J. Come, M. A. Lowe, J. W. Kim, P. Taberna, S. H. Tolbert, H. D. Abruna, P. Simon and B. Dunn, *Nat. Mater.*, 2013, **12**, 518.
34 T. Brezesinski, J. Wang, S. H. Tolbert and B. Dunn, *Nat. Mater.*, 2010, **9**, 146.

